International Journal of Wireless Information Networks, Vol. 14, No. 2, June 2007 (© 2006)
DOI: 10.1007/s10776-006-0046-x

Dirty RF: A New Paradigm

Gerhard Fettweis,[1,2] Michael Löhning,[1] Denis Petrovic,[1] Marcus Windisch,[1] Peter Zillmann,[1] and Wolfgang Rave[1]

The implementation challenge for new low-cost low-power wireless modem transceivers has continuously been growing with increased modem performance, bandwidth, and carrier frequency. Up to now we have been designing transceivers in a way that we are able to keep the analog (RF) problem domain widely separated from the digital signal processing design. However, with today's deep sub-micron technology, analog impairments – "dirt effects" – are reaching a new problem level which requires a paradigm shift in the design of transceivers. Examples of these impairments are phase noise, non-linearities, I/Q imbalance, ADC impairments, etc. In the world of "Dirty RF" we assume to design digital signal processing such that we can cope with a new level of impairments, allowing lee-way in the requirements set on future RF sub-systems. This paper gives an overview of the topic and presents analytical evaluations of the performance losses due to RF impairments as well as algorithms that allow to live with imperfect RF by compensating the resulting error effects using digital baseband processing.

KEY WORDS: Dirty RF; apperture and clock jitter; phase noise; I/Q imbalance; non-linear PA

1. INTRODUCTION

Wireless communications systems have seen a rapid development in recent years, with an approximate ten-fold increase in data rates every 5 years. Current research and standardization efforts indicate that this trend is bound to continue – aiming at data rates above 1 GBit/s (short range) and 100 MBit/s (cellular) for next generation wireless networks. Developing these systems not only requires to steadily increase spectral efficiency and ever closer approach *physical* limits, i.e., the Shannon bound; it also calls for techniques to approach *engineering Shannon bounds* – the technological limits set by analog RF front-ends. The true test of the practicality of any communication system design is the performance of the system when taking into account the impairments of analog RF components.

This paper reviews some of the most important impairments limiting the performance of future wireless communications, namely: aperture and clock jitter, phase noise, I/Q imbalance, non-linearity of the high power amplifier. Algorithms that allow for compensation of these impairments by digital baseband processing are also presented.

Jitter – aperture jitter as well as clock jitter – is the limiting effect for high speed analog-to-digital converters (ADCs) with high resolution and wide digitization bandwidth, which are required in receivers in order to support high data rates. Section 2 presents an explicit analysis of both the aperture jitter and the clock jitter effects for arbitrary stationary input signals in terms of SNR and error spectra at the ADC output.

The performance of an OFDM system can be strongly degraded by the presence of random *phase noise* in oscillators, especially if a system design targets high data rates at high carrier frequencies. If imperfect oscillators are used in an OFDM system, they will influence the transmission by two effects that

[1] Vodafone Chair Mobile Communications Systems, Technische Universität Dresden, D-01062, Dresden, Germany
[2] E-mail: fettweis@ifn.et.tu-dresden.de

occur due to phase noise: rotation of all demodulated subcarriers of an OFDM symbol by a random common angle, called common phase error (CPE) and the occurrence of intercarrier interference (ICI). In this paper, we present an algorithm for intercarrier-interference mitigation. Simulation results show the effectiveness of the presented algorithm in Section 3.

I/Q processing architectures avoid the need for bulky analog image rejection filters, enabling highly reconfigurable and cost-efficient terminals. However, unavoidable imbalances between the I- and Q-branch lead to a limited image attenuation. Section 4 introduces an *I/Q imbalance* compensation scheme in which the unknown analog imbalance parameters are estimated digitally without the need for any calibration or training signal allowing for the interference by the image signal to be effectively compensated.

Section 5 considers a major drawback of OFDM and superimposed CDMA signals – the high dynamic range of the transmit signal. The transmit Power Amplifier (PA) and other elements in the signal path have to be operated at high Input Power Backoff (IBO), which decreases the efficiency of the PA and leads to high costs. We present a powerful receive algorithm for OFDM signals transmitted over a *nonlinear PA*.

In total, this paper gives an introduction into the modeling of RF impairments and of first results of "Dirty RF" receiver techniques.

2. APERTURE JITTER AND CLOCK JITTER

The interface between the analog domain and the digital domain is one of the most critical functionalities in the analog frond end of modern wireless modem transceivers. Unfortunately, the performance (i.e., the resolution bandwidth product) of ADCs is strongly limited by technology dependent physical error effects like thermal circuit noise, comparator ambiguity, and jitter [1]. As is commonly known, especially jitter – aperture jitter as well as clock jitter – drastically reduces the achievable signal-to-noise ratio (SNR) of ADCs [1–9]. Although the SNR limiting effect of aperture jitter and clock jitter is quite similar, there also exist significant differences between the resulting jitter-induced error processes at the ADC output. These differences seem to be not commonly known and are often neglected by simple jitter models, respectively.

In the following we present a general analysis of the effects of sampling jitter in ADCs, which holds for arbitrary stationary input signals and comprises aperture jitter effects as well as clock jitter effects. Additionally to SNR formulas, also expressions for the corresponding error spectra at the ADC output are derived. The presented results enable developers of new receiver concepts to model jitter-induced error effects in the ADC in an adequate manner. Thus, it becomes easier to decide if and by which means jitter effects in the ADC can be compensated.

2.1. Sampling with Jitter

In order to obtain general results independent of a special (possibly unknown) input signal phase spectrum, we consider a wide-sense stationary (WSS) random process $s(t)$ at the ADC input [6–8]. $s(t)$ shall be given by its Fourier series expansion [10]

$$s(t) = \sum_{i=-\infty}^{\infty} \underbrace{\underline{c}_i \mathrm{e}^{\mathrm{j}\,2\pi f_i t}}_{s_i(t)}$$

$$\text{with } \mathrm{E}\{\underline{c}_i \underline{c}_k^*\} = \begin{cases} |\underline{c}_i|^2 & \text{if } i = k \\ 0 & \text{else} \end{cases} \tag{1}$$

In the ADC $s(t)$ is sampled at the time instants $t_n = nT + J_n$ with the nominal sampling period T. J_n denotes the random sampling time variations caused by the random jitter process. The effect of these sampling time variations are random amplitude errors in the ADC output signal. The resulting mean error power measured over a block of N samples can be calculated as follows [6–9]

$$P_J = \frac{1}{N} \sum_{n=0}^{N-1} \sum_{i=-\infty}^{\infty} 2|\underline{c}_i|^2 \left(1 - \mathrm{E}\left\{e^{\mathrm{j}2\pi f_i J_n}\right\}\right) \tag{2}$$

where $\mathrm{E}\left\{e^{\mathrm{j}2\pi f_i J_n}\right\}$ is the characteristic function of the overall jitter process. So far only periodic input signals with a line spectrum have been considered. The extension to non-periodic signals with a continuous power spectral density (psd) $S_{ss}(f)$ yields [6–8]

$$P_J = \frac{1}{N} \sum_{n=0}^{N-1} 2 \int_{-\infty}^{\infty} S_{ss}(f) \left(1 - \mathrm{E}\left\{e^{\mathrm{j}2\pi f J_n}\right\}\right) \mathrm{d}f$$

The signal power is given by the integral over $S_{ss}(f)$. Hence, the jitter dependent SNR (in decibels) is

$$\mathrm{SNR_J} = 10 \lg \left(\frac{\int_{-\infty}^{\infty} S_{ss}(f)\,\mathrm{d}f}{P_\mathrm{J}} \right) \mathrm{dB} \tag{3}$$

Not only the mean sampling error power has to be considered for a complete description of the effects of sampling jitter in ADCs, but also its spectral

distribution, i.e., the corresponding error power spectrum $S_{ee}(e^{j2\pi fT})$ at the ADC output. Using the stochastic input signal model described by (1), the following expression can be derived for the error auto-correlation function at the ADC output.

$$s_{ee}(nT, mT) = \sum_{i=-\infty}^{\infty} |c_i|^2 e^{j2\pi f_i(n-m)T} \cdot \left[1 + E\left\{e^{j2\pi f_i(J_n - J_m)}\right\} - E\left\{e^{j2\pi f_i J_n}\right\} - E\left\{e^{-j2\pi f_i J_m}\right\}\right] \quad (4)$$

As can be seen, the error auto-correlation function depends on the characteristic functions $E\{e^{j2\pi f J_n}\}$ and $E\{e^{-j2\pi f J_m}\}$ of the overall jitter process at the sampling time instants nT, mT and of the characteristic function $E\{e^{j2\pi f(J_n - J_m)}\}$ of the difference $J_n - J_m$. Before transforming (4), i.e., calculating the corresponding error power spectrum, it is useful to analyze $E\{e^{j2\pi f J_n}\}$, $E\{e^{-j2\pi f J_m}\}$, and $E\{e^{j2\pi f(J_n - J_m)}\}$ for the different kinds of jitter.

2.2. Jitter Models

Aperture jitter stands for the random sampling time variations in ADCs which are caused by broadband noise in the sample-&-hold circuit. It is commonly modeled as a stationary white Gaussian process [1–3], i.e., the corresponding sampling time variations $J_n^{ap} = t_n - nT$ are assumed to be independent identically distributed (i.i.d.) Gaussian random variables with zero mean and the variance σ_{ap}^2. Hence, the characteristic functions of J_n^{ap} and $J_n^{ap} - J_m^{ap}$ are

$$E\left\{e^{\pm j2\pi f J_n^{ap}}\right\} = E\left\{e^{\pm j2\pi f J_m^{ap}}\right\} = e^{-2\pi^2 f^2 \sigma_{ap}^2} \quad (5)$$

and

$$E\left\{e^{j2\pi f(J_n^{ap} - J_m^{ap})}\right\} = \begin{cases} 1 & \text{if } n = m \\ \left[e^{-2\pi^2 f^2 \sigma_{ap}^2}\right]^2 & \text{if } n \neq m \end{cases} \quad (6)$$

Clock jitter is a property of the clock generator that feeds the ADC with the clock signal. It is caused by the phase noise of the oscillator and generates additional sampling time errors in the ADC. In [11], it is shown that the phase noise of free running oscillators can be modeled as a Wiener process, i.e., a continuous-time *non-stationary* random process with independent Gaussian increments. Time-discretization of the Wiener process yields the model of accumulated timing-jitter commonly used for the clock jitter [3, 12], where the sampling time variations J_n^{acc} are modeled as

$$J_0^{acc} \doteq 0 \quad \text{and} \quad J_n^{acc} = \sum_{i=1}^{n} \delta_i$$

The jitter increments δ_i are i.i.d. Gaussian random variables with zero mean and the variance $\sigma_{\delta_i}^2 = cT$. Here c stands for the phase noise constant of the oscillator (defined in [11]) and T for the nominal clock period. The product cT of the phase noise constant and the nominal clock period is the so-called cycle jitter variance. Its square root $\sqrt{cT}$ is a typical parameter of clock generators known as the rms cycle jitter. Using the accumulated jitter model the following expressions for the characteristic jitter functions can be derived

$$E\left\{e^{\pm j2\pi f J_n^{acc}}\right\} = \left[E\left\{e^{j2\pi f \delta_1}\right\}\right]^n = e^{-2\pi^2 f^2 cnT} \quad (7)$$

and

$$E\left\{e^{j2\pi f(J_n^{acc} - J_m^{acc})}\right\} = e^{-2\pi^2 f^2 cT|n-m|} \quad (8)$$

It should be noted that in the case of clock jitter the characteristic functions depend on the absolute sampling time while in the case of aperture jitter they are time-invariant.

2.3. Aperture Jitter versus Clock Jitter Effects

By means of the jitter models presented in Section 2 the error effects caused by aperture and by clock jitter shall be compared. The overall SNR as well as the spectral distribution of the mean error power will be considered.

2.3.1. Comparison of The Overall SNR

Substituting the characteristic jitter functions given by (5) and (7) into (3) yields the values SNR_{ap} and SNR_{acc} for aperture jitter SNR and clock jitter SNR, respectively. In the case of aperture jitter the SNR is independent of the number of sampling points N, while in the case of clock jitter the SNR strongly depends on it [6–8] (results not shown).

In Figure 1, the SNR formulas are evaluated for a fixed sampling block length of 1 ms, a 50 MHz sine wave as an input signal, a sampling frequency of 100 MHz, and the given jitter parameters. The solid curves represent the results for a sinusoidal input signal with the specified frequencies. The dashed curves are calculated for a band-limited white noise

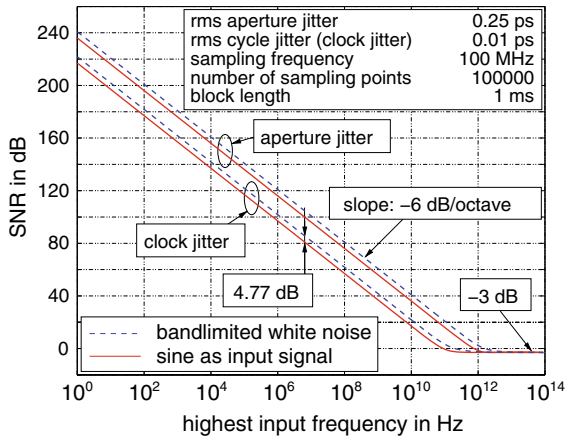

Fig. 1. Comparison of the SNR caused by aperture and clock jitter for a sinusoidal input signal and a bandlimited white noise input with different signal/cut-off frequencies.

input with different cut-off frequencies. One can see that the SNR trends are, in principle, the same for both kinds of jitter as well as for both kinds of input signals. The SNR decreases with about 6 dB per doubling the input frequency or bandwidth (which is equivalent to a loss of 1 bit of ADC resolution) and converges to −3 dB if the highest input frequency exceeds the inverse rms (root mean square) jitter values σ_{ap}^{-1} and $1/\sqrt{cNT}$. The following can be concluded:

(1) The SNR is mainly determined by the highest frequency components of the input signal and less by its bandwidth.
(2) Although the absolute SNR values strongly depend on the jitter parameters of the ADC and the clock generator in connection with the specific sampling block length, the effect of aperture and clock jitter on the overall SNR is, in principle, the same.

2.3.2. Comparison of the Error Power Spectra

In order to obtain expressions for the error power spectra caused by the different jitter processes, the corresponding error auto-correlation functions $s_{ee_{\text{ap}}}$ and $s_{ee_{\text{acc}}}$ have to be derived and transformed by means of the DTFT. In [6–8] it was shown that in cases where the maximum input signal frequency $f_{i_{\max}}$ is very low compared to the inverse of the rms jitter value σ_{ap} (which holds for the majority of applications), the error power spectrum for the case of **aperture jitter** can be approximated by

$$S_{ee_{\text{ap}}}\left(e^{\mathrm{j}2\pi fT}\right) \approx \sum_{i=-\infty}^{\infty} 2|\underline{c}_i|^2 \cdot g_i = \text{const} \tag{9}$$

Equation (9) proves the common assumption that the mean error power caused by aperture jitter (in most cases) is equally distributed over the whole digitization band ($-1/2T < f < 1/2T$), which motivates the approach to increase the jitter dependent SNR in a given frequency band by means of oversampling and filtering.

For the case of *clock jitter* the error auto-correlation function does not only depend on the sampling time difference $kT = (n-m)T$ but also on the absolute sampling time instants. In order to model the corresponding error power spectrum one can use the following approach. For each sampling time instant nT a short-time error power spectrum is calculated. The observation period is determined by the sampling block length NT, which should not be too small in order to reduce windowing effects. The resulting spectra can be interpreted as a time-varying power spectrum $S_{ee_{\text{acc}}}\left(e^{\mathrm{j}2\pi fT}, nT\right)$ in the sense of a discrete-time Rihaczek spectrum [13–15]. Hence, the time average

$$\overline{S}_{ee_{\text{acc}}}\left(e^{\mathrm{j}2\pi fT}\right) = \frac{1}{N}\sum_{n=0}^{N-1} S_{ee_{\text{acc}}}\left(e^{\mathrm{j}2\pi fT}, nT\right) \tag{10}$$

is supposed to be a meaningful measure of the spectral distribution of the mean error power. For sufficiently long observation intervals NT the time-averaged error power spectrum can be approximated by [7, 8]

$$\bar{S}_{ee_{\text{acc}}}\left(e^{\mathrm{j}2\pi fT}\right) \approx \underbrace{\frac{1}{T}\sum_{l=-\infty}^{\infty}\delta\left(f-\frac{l}{T}\right)}_{\text{spectral repetition}} * \left[\sum_{i=-\infty}^{\infty}\underbrace{|\underline{c}_i|^2\delta(f-f_i)\cdot\tilde{g}_i}_{\text{weighted lines of the input psd}} + \sum_{i=-\infty}^{\infty}|\underline{c}_i|^2\underbrace{\frac{f_i^2 c}{\pi^2 f_i^4 c^2+(f-f_i)^2}}_{\text{Lorentzian spectrum}}\right] \tag{11}$$

with the spectral gain coefficients

$$\tilde{g}_i = \frac{1}{N}\sum_{n=0}^{N-1}\left(1-\mathrm{e}^{-2\pi^2 f_i^2 cnT}\right) \tag{12}$$

which are specific for each spectral component of the input signal. It can be stated that the error power spectrum caused by accumulated clock jitter consists

of two significantly different parts. The first part comprises the lines of the input psd weighted with the spectral gains $\tilde{g}_i$. The second part is composed by Lorentzian shaped spectra centered around the frequencies f_i of the input signal components. This means that the corresponding error power is strongly concentrated around the frequency components of the input signal. Moreover, as can be seen from (11), the error power concentrated in a certain line component at the frequency f_i is determined by the power $|\underline{c_i}|^2$ of the corresponding input signal component multiplied with the spectral gain $\tilde{g}_i$. Since the spectral gains $\tilde{g}_i$ significantly increase as the frequencies f_i increase (see (12)), higher frequency signal components are more disturbed than lower ones. This is a significant difference to the aperture jitter effect where the greatest part of the error power is equally distributed over the whole digitization band. It can be concluded that the error noise caused by clock jitter is highly correlated. Consequently, the clock jitter dependent SNR cannot be increased by oversampling techniques.

3. PHASE NOISE

3.1. System Model

As mentioned in the Introduction, phase noise mainly poses a problem for OFDM because it destroys orthogonality among the subcarriers [16]. Assuming OFDM transmission with perfect frequency and timing synchronization, OFDM signal samples, sampled at frequency f_s at the receiver, in the presence of phase noise can be expressed as $r(n) = (x(n) * h(n))\, e^{j\phi(n)} + \xi(n)$. Frequency offset is also covered by this model. Each OFDM symbol is assumed to consist of a cyclic prefix of length N_{CP} samples and N samples corresponding to the useful signal. The variables $x(n)$, $h(n)$ and $\phi(n)$ denote the time domain samples of the transmitted signal, the channel impulse response and the phase noise process at the output of the mixer, respectively. The symbol * stands for convolution. The term $\xi(n)$ represents AWGN noise with variance σ_n^2.

The phase noise process $\phi(t)$ represents the phase deviation at the output of the frequency synthesizer, which is for simplicity here modeled as a Wiener process [11]. As in Section 2.2 a characteristic constant c is used to scale an accumulated Gaussian random variable which is related to the 3 dB bandwidth of the Lorentzian spectrum associated with the Wiener process by $\Delta f_{3\text{dB}} = \pi f_c^2 c$ with f_c being the carrier frequency. Note, however, that all results in this section can be applied to a general phase noise model. To characterize the quality of an oscillator in an OFDM system the relative phase noise bandwidth $\delta_{PN} = \Delta f_{3\text{dB}}/\Delta f_{car}$ is used, where Δf_{car} is the subcarrier spacing.

At the receiver after removing the N_{CP} samples corresponding to the cyclic prefix and taking the discrete Fourier transform (DFT) on the remaining N samples, the demodulated carrier amplitudes R_s at subcarrier s $(s = 0, 1, \ldots N-1)$ of one OFDM symbol are given as:

$$R_s = X_s H_s \underbrace{J(0)}_{\text{CPE}} + \underbrace{\sum_{\substack{v=0 \\ v\neq s}}^{N-1} X_v H_v J(s-v)}_{\text{ICI}} + \eta_s \qquad (13)$$

where X_s, H_s and η_s represent transmitted symbols on the subcarriers, the sampled channel transfer function at subcarrier frequencies and transformed white noise which remains AWGN with variance σ_n^2. The terms $J(i)$ $i = -N/2, \ldots, N/2-1$ represent the DFT of the realization of the process $e^{j\phi(n)}$ during the current OFDM symbol, thus indirectly representing the spectrum of the process.

The term $J(0)$ does not depend on the subcarrier index and modifies all subcarriers of one OFDM symbol in the same manner. Thus it is referred to in the literature as the CPE [16]. The CPE term is usually estimated using pilots [17, 18] and corrected for by constellation derotation. However, the residual error due to ICI can also be large [19], thus ICI suppression methods need to be addressed. In this paper, we present an algorithm for ICI mitigation.

3.2. Phase Noise Approximation and Correction

3.2.1. ICI Correction – Basic Idea

A phase noise compensation beyond the simple CPE correction will be possible only if one knows the instantaneous realization of the phase noise process. The already introduced factors $J(i)$, $i = -N/2, \ldots, N/2-1$ represent the DFT coefficients (spectral components) of one realization of the random process $e^{j\phi(n)}$. The more spectral components $J(i)$ of the signal are known, the more is known of the signal waveform $e^{j\phi(n)}$, and thus $\phi(n)$. The signal $e^{j\phi(n)}$ has the characteristics of a low-pass signal [11], with psd of the form $1/(1 + f^2)$, where f denotes the frequency offset w.r.t. the carrier. Additionally, phase noise has a very small bandwidth compared with the subcarrier spacing. Due to the shape of the spectrum of $e^{j\phi(n)}$,

very few low pass spectral components in most cases suffice to give a "good" approximation of the phase noise waveform (realisation). This is illustrated by the example in Figure 2, where it can be seen that already the second order approximation gives a much better phase noise approximation than only the DC value. Therefore, knowledge of the coefficients $J(i)$ gives the possibility to approximate the phase noise waveform to a higher order, and allows a better compensation of it than with only CPE correction, i.e., the 0th order approximation.

3.2.2. ICI Correction Algorithm

The details of an ICI suppression algorithm can be found in our previous work [19, 20]. The proposed ICI suppression algorithm estimates as many spectral components $J(i)$, $i = -N/2, \ldots, N/2-1$ as possible using MMSE estimation. The information about these spectral components is hidden in the ICI part of the signal at the output of the DFT demodulator with R_s, $s = 0, 1, \ldots N-1$ given by Eq. (13). The estimation algorithm is a decision feedback algorithm, since it requires knowledge of transmitted symbols. As transmitted symbol estimates, the symbols after initial CPE correction are adopted. Once the DFT coefficients of the phase noise are known, one possesses enough information about the phase noise waveform to suppress it at least to a certain degree beyond the standard CPE compensation.

Phase noise suppression in the time domain would be a logical approach by multiplying the received signal $r(n) = (x(n) * h(n))e^{j\phi(n)} + \xi(n)$ with the conjugate of the estimated phase noise process $e^{-j\phi(n)}$. However, multiplication in time domain for discrete time systems can be mapped to a circular convolution of DFT spectra in the frequency domain [21]. This avoids two FFT transforms and means that ICI cancellation for the current OFDM symbol can be done in the frequency domain by circularly convolving the demodulated symbols vector of all subcarriers $\mathbf{R}_N = [R(0), \ldots, R(N-1)]^{\mathrm{T}}$ with the vector of estimated DFT coefficients of $e^{-j\phi(n)}$.

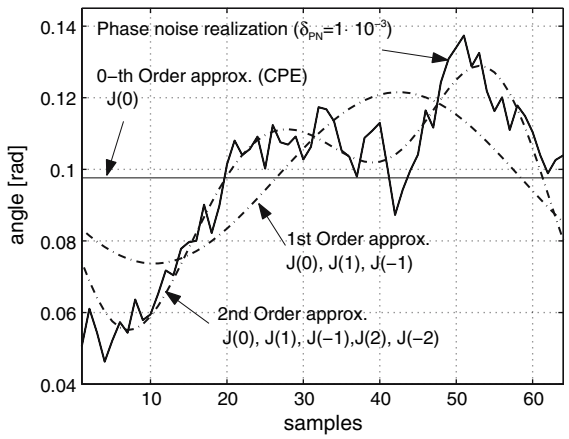

Fig. 2. Phase noise waveform approximation using various orders of approximation.

The concrete realization of an algorithm is as follows:

(1) *Step 1*: Perform standard CPE correction using least squares (LS) estimation [17, 18].
(2) *Step 2*: Make a decisions on the transmitted symbols and use all available hard decisions for the MMSE estimation of the $J(i)$, $i = -u \ldots u$, according to the method provided in [20]. Here u denotes the order of the phase noise approximation.
(3) *Step 3*: Convolve the vector of the received symbols with the DFT coefficients of the *conjugate* of the phase noise waveform.

3.2.3. Iterative Phase Noise Suppression

The above described algorithm for ICI suppression is a decision feedback algorithm and therefore subject to error propagation. It is to be expected that falsely detected symbols after initial CPE correction, which are fed to the MMSE estimator in *Step 2* of the algorithm, reduce the estimation quality of the DFT coefficients of the phase noise process. Thus the reduction of the symbol error rate of the symbols, which are fed back, should improve the performance of the phase noise suppression. This can be achieved if the algorithm described in Section 3.2.2 is applied iteratively instead of just once.

A block diagram to implement this scheme is presented in Figure 3.

The proposed algorithm is realized in three steps:

(1) *Step 1*: Perform standard CPE correction using least square (LS) estimation [17, 18].
(2) *Step 2*: Carry out the ICI suppression algorithm described in the previous section (only *Steps* 2 and 3). Switch is in position 1,
(3) *Step 3*: Demodulate QAM symbols and feed them back to the Step 2. Turn the switch to position 2. Iterate until the desired number of iterations is reached.

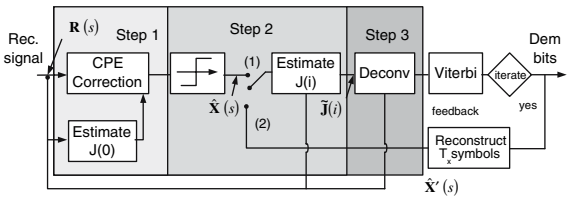

Fig. 3. Block diagram of the iterative phase noise suppression algorithm.

The complexity of the algorithm is large, however the performance of the algorithm is significantly improved as will be shown in Section 3.3.

3.3. Numerical Results

In order to investigate the performance of the proposed algorithm we resort to Monte Carlo simulations. System parameters correspond to the IEEE802.11a standard [22], i.e., 48 useful carriers, four pilot symbols and 64-QAM. Further, a convolutional code of rate $r = 1/2$ and a Viterbi decoder are used. We assumed 10 OFDM symbols per packet. Within the simulations six phase noise correction schemes are compared:

(1) without phase noise
(2) phase noise with ideal CPE correction (ICPE)
(3) phase noise with CPE correction using the least squares (LS) algorithm according to [18]
(4) phase noise with genie ICI correction of order $u = 3$
(5) phase noise with one-step ICI correction (0 iterations) of order $u = 3$
(6) phase noise and iterative ICI correction.

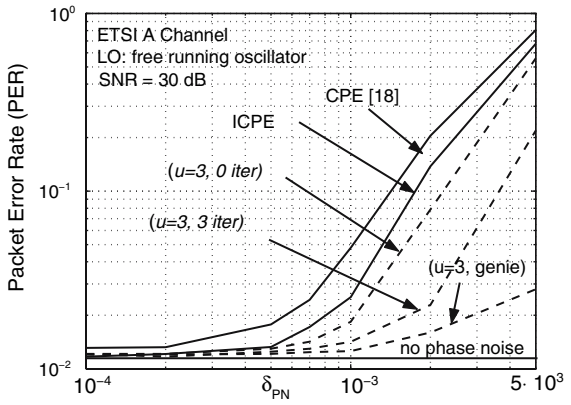

Fig. 4. Free-running oscillator with different correction schemes.

We investigated the performance of the algorithms for frequency selective channels and a free running oscillator. The dependence of the packet error rate PER on varying phase noise bandwidth δ_{PN} for a free-running oscillator is plotted in Figure 4 for one example of a frequency selective channel (ETSI A channel). The PER of 10^{-2} was selected as a reference. The non-iterative ICI correction algorithm shows better performance than the pure CPE correction. We also observe, that the iterative algorithm performs much closer to the genie ICI correction then the single-step approach.

The iterative algorithm provides results that are roughly one order of magnitude better in terms of PER than simple CPE suppression. A further increase of the approximation order did not improve performance for our parameters, due to the fact that not enough equations (known data symbols) are available. For a larger number of subcarriers (longer symbol duration) this would have to be adapted.

4. I/Q IMBALANCE

I/Q signal processing receiver architectures, such as the direct conversion receiver [23] and the low-IF receiver [24], are of great value for reconfigurable and low-cost radio applications. Since no fixed analog image rejection filter is needed, such architectures allow low-cost and highly flexible analog front-ends. In theory, an infinite image rejection is provided, if the complex analog oscillator has equal amplitudes and a phase difference of exactly 90° in the I- and the Q-branch of the signal processing path. However, a perfect match between the I- and the Q-branch is not feasible in a hardware implementation due to the limited accuracy of the analog components. These unavoidable mismatches, known as I/Q imbalance, significantly degrade the image rejection capability of any I/Q signal processing architecture.

The limited image attenuation is a major concern in low-IF receivers. Here the so called image signal is separated from the desired signal by twice the intermediate frequency (IF). In the presence of a powerful image signal, the image attenuation provided by the analog I/Q signal processing alone is not sufficient. The direct conversion receiver is generally more robust against powerful adjacent channels. However, the degrading effect of the I/Q imbalance persists. This holds in particular, if the signal of interest is a multicarrier signal (such as OFDM) transmitted over a frequency-selective fading channel.

Different concepts for the digital correction of the I/Q imbalance are under active research. An appropriate calibration, i.e., an accurate estimation of the unknown parameters of the I/Q imbalance, is challenging. The conventional way of calibration is characterized by an injection of some kind of known signals to the RF part of the receiver. Typical approaches include an off-line calibration using analog test signals [25, 26], and techniques for the reception of dedicated signals with inherent pilots [27]. However, such "knowledge-dependent" approaches come with specific drawbacks [28, 29]. It will be shown in this section, that a completely "blind" I/Q imbalance parameter estimation and compensation is feasible. The presentation will be focused on the direct conversion receiver. However, the fundamental concept of the blind parameter estimation is also applicable to alternative I/Q processing architectures, such as the low-IF receiver [28].

4.1. I/Q Imbalance in OFDM Direct-Conversion Receivers

The fundamental principle of the direct-conversion architecture is to multiply the received RF signal with two orthogonal phases of a local oscillator (LO) signal, where the frequency of the LO f_{LO} is chosen equal to the carrier frequency of the desired RF signal. Ideally, the complex LO signal has the time function $x_{\mathrm{LO}}(t) = e^{-j2\pi f_{\mathrm{LO}}t}$, which corresponds to the desired down-conversion by f_{LO}. The I/Q imbalance due to an imperfect implementation can be modeled by a complex LO signal with the time function $\tilde{x}_{\mathrm{LO}}(t) = \cos(2\pi f_{\mathrm{LO}}t) - jg\sin(2\pi f_{\mathrm{LO}}t + \varphi)$, where g denotes the amplitude imbalance and φ denotes the phase imbalance. Based on g and φ, the complex valued I/Q imbalance parameters

$$K_1 = \frac{1 + ge^{-j\varphi}}{2}, \quad K_2 = \frac{1 - ge^{+j\varphi}}{2} \tag{14}$$

are defined, in order to rewrite the time function of the complex LO with I/Q imbalance as

$$\tilde{x}_{\mathrm{LO}}(t) = K_1 e^{-j2\pi f_{\mathrm{LO}}t} + K_2 e^{+j2\pi f_{\mathrm{LO}}t}. \tag{15}$$

Therefore, direct-conversion with I/Q imbalance can be interpreted as a superposition of a desired down-conversion (weighted by K_1) and an undesirable up-conversion (weighted by K_2). The impact of the I/Q imbalance on the transmitted baseband signal depends on the internal structure of the baseband signal. It has been shown in [29] that the receiver I/Q imbalance translates to a mutual interference between symmetric subcarriers in OFDM systems (see Figure 5). Using matrix notation, this mutual interference can be efficiently modeled by

$$\begin{bmatrix} Z_m(n) \\ Z^*_{-m}(n) \end{bmatrix} = \mathbf{K} \begin{bmatrix} Y_m(n) \\ Y^*_{-m}(n) \end{bmatrix}, \quad \mathbf{K} = \begin{bmatrix} K_1 & K_2 \\ {K_2}^* & {K_1}^* \end{bmatrix}, \tag{16}$$

where the asterisk $(\cdot)^*$ denotes complex conjugation. Throughout this section, the subscript m denotes the subcarrier index and the argument n denotes the sample time index of the OFDM symbols. For example, $Z_m(n)$ denotes the demodulated symbol at the mth subcarrier of the nth OFDM symbol. In order to concisely model the effects of the I/Q imbalance effects, the interval of subcarrier indices is set to $m \in [-L_{\mathrm{DFT}}/2;\ L_{\mathrm{DFT}}/2-1]$, where L_{DFT} denotes the order of the DFT. The index $m = 0$ corresponds to the DC subcarrier.

The symbols $Y_m(n)$ correspond to the equivalent baseband signal of the received RF signal before down-conversion (see Figure 5). In the case of an imbalance-free I/Q down-conversion ($K_1 = 1$, $K_2 = 0$), these symbols will appear at the output of the OFDM demodulator: $Z_m(n) = Y_m(n)$. The key for a digital compensation of the I/Q imbalance lies in the so called mixing matrix $\mathbf{K}$. Because $\mathbf{K}$ is always non-singular for realistic imbalance parameters, the desired OFDM symbols $Y_m(n)$ and $Y_{-m}(n)$ can be perfectly reconstructed out of the interfered symbols $Z_m(n)$ and $Z_{-m}(n)$ using the inverse $\mathbf{K}^{-1}$.

It should be stressed, that the desired symbols $Y_m(n)$ are not necessarily identical to the transmitted symbols $X_m(n)$. Instead, $Y_m(n)$ might be corrupted

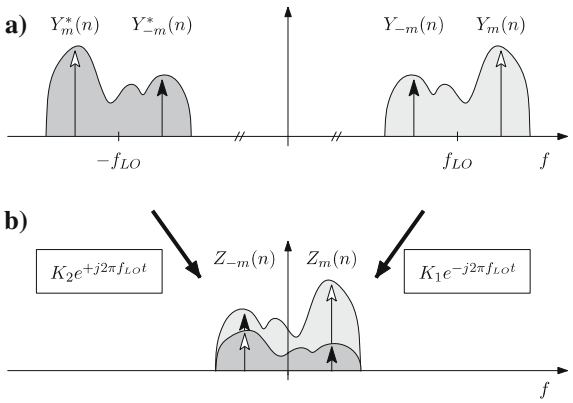

Fig. 5. Frequency domain illustration of I/Q imbalance in OFDM direct-conversion receivers: (a) Spectrum of the real-valued RF signal, (b) Spectrum of the complex-valued baseband signal.

by the channel or by other RF impairments. For example, the previous section addressed errors in the absolute phase of the LO signal due to phase noise. Similarly, carrier frequency offset is an important issue in practical implementations. However, the effect of these distortions can be *separated* from the I/Q imbalance effects [30]. This property motivates the approach of a successive compensation of the different impairments.

In this section, we focus on the reconstruction of $Y_m(n)$, i.e., the goal is to provide OFDM symbols equivalent to those of a perfectly balanced I/Q down-conversion. The compensation of additional impairments required for reconstructing the transmitted symbols $X_m(n)$ is conveyed to arbitrary subsequent signal processing techniques, such as those presented in other sections of this paper.

4.2. Blind I/Q Imbalance Parameter Estimation

It has been shown in [29] that a completely blind estimation of the I/Q imbalance parameters is possible. The rationale of this novel approach is, that the unknown product $K_1\ K_2$ is determined by the statistics of the interfered symbols:

$$K_1 K_2 = \frac{\mathrm{E}\{Z_m(n) Z_{-m}(n)\}}{\mathrm{E}\left\{|Z_m(n) + Z^*_{-m}(n)|^2\right\}}, \qquad (17)$$

where $\mathrm{E}\{\cdot\}$ denotes expectation. The only assumption that was introduced is, that $\mathrm{E}\{Y_m(n) Y_{-m}(n)\} = 0$ holds at the examined subcarrier index m. In other words, the symbols of at least one pair of symmetric subcarriers $Y_m(n)$ and $Y^*_{-m}(n)$ must be uncorrelated and have zero mean. In practical OFDM systems this assumption is realistic at least for pairs of data-subcarriers, if a proper source and channel coding is applied.

In a practical receiver implementation, the expectation terms of (17) have to be replaced by sample based approximations. This can be done by an averaging operation over multiple pairs of uncorrelated subcarriers. Furthermore, the I/Q imbalance parameters change very slowly with time. Hence, an averaging over time is also reasonable. The estimation can be formally written as

$$\hat{K}_1 \hat{K}_2 = \frac{\sum_{m \in M} \sum_{n \in N} Z_m(n) Z_{-m}(n)}{\sum_{m \in M} \sum_{n \in N} |Z_m(n) + Z^*_{-m}(n)|^2}. \qquad (18)$$

M denotes the chosen subset of M (positive) subcarrier indices, N denotes the chosen subset of N sample time indices. Obviously, the accuracy of the estimation will be affected by the number of incorporated sample pairs $M\ N$. An increased subcarrier block size M raises the computational effort at each time instant n, whereas an increased temporal block size N raises the duration of the parameter estimation. Hence, the proposed parameter estimation allows for a flexible tradeoff between accuracy, computational effort and measurement time.

Based on the estimated product $\hat{K}_1 \hat{K}_2$ an estimate of the inverse $\hat{\mathbf{K}}^{-1}$ can be derived [29, 31]. Using this blindly gained compensation matrix, a reconstruction of the desired symbols is possible:

$$\begin{bmatrix} \hat{Y}_m(n) \\ \hat{Y}^*_{-m}(n) \end{bmatrix} = \hat{\mathbf{K}}^{-1} \begin{bmatrix} Z_m(n) \\ Z^*_{-m}(n) \end{bmatrix} = \hat{\mathbf{K}}^{-1} \mathbf{K} \begin{bmatrix} Y_m(n) \\ Y^*_{-m}(n) \end{bmatrix}. \qquad (19)$$

Note, that the estimation of the compensation matrix $\hat{\mathbf{K}}^{-1}$ is restricted to uncorrelated pairs of symmetric subcarriers. In contrast, the subsequent compensation (19) can be applied to all subcarrier indices m.

4.3. Simulation Results

The capabilities of the proposed I/Q imbalance compensation algorithm has been studied considering the IEEE 802.11a WLAN standard [32], which is a widely used OFDM-based wireless communications standard. A detailed performance analysis can be found in [29, 31]. Exemplarily, Fig. 6 shows the resulting symbol error rate (SER) for a frequency-selective fading channel. The I/Q imbalance parameter estimation is done based on all data-subcarriers, which results in $M = 24$ for the IEEE 802.11a signal [32]. The performance-degrading impact of the I/Q imbalance is clearly visible. Even for a high SNR the SER never falls below a specific limit, which is predetermined by the parameters of the I/Q imbalance (here: 5.3% SER for $g = 1.05$, $\phi = 5°$). Such a lower limit still exists if the proposed compensation is applied. However, depending on the requirements of the chosen communications standard, the error floor can be arbitrarily decreased by a proper choice of the block size N. For example, a block size of $N = 100$ (equivalent to 0.4 ms measurement time) is sufficient for reaching a SER of 0.2 %.

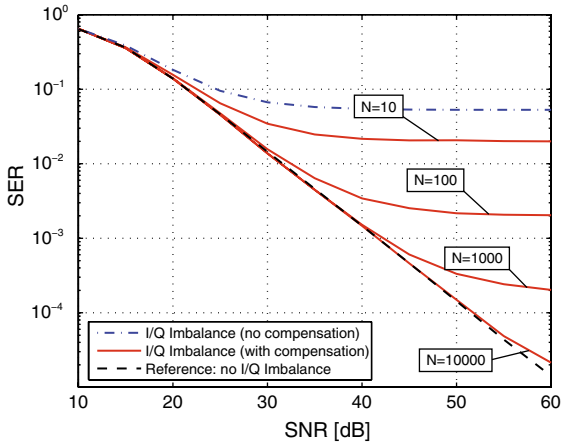

Fig. 6. Mean symbol error rate for an ETSI-A channel and I/Q imbalance parameter estimation based on all data-subcarriers (64-QAM, $g = 1.05$, $\phi = 5°$).

4.4. Outlook

The concept of a completely blind on-line estimation and compensation of the I/Q imbalance has shown to be a feasible approach in common OFDM systems. While being generally independent from the existence of any known symbols, the performance of the parameter estimation can be improved in the presence of standard specific pilots [31]. This useful property can be utilized to design training symbols suited for both channel estimation and I/Q imbalance estimation [30]. An extension of the proposed technique towards frequency-selective I/Q imbalance is under active research.

5. NON-LINEAR POWER AMPLIFIER

The time-domain signal in an OFDM data transmission system is the superposition of many carriers by means of an *Inverse Discrete Fourier Transform* (IDFT). This results in an approximately Gaussian distribution of the I- and Q-components of the complex baseband signal [33]. Consequently, OFDM systems require transmit and receive signal processing blocks with a high dynamic range, which leads to costly RF components. The high *Peak-to-Average Power Ratio* (PAPR) of the OFDM transmit signal is especially problematic for the PA [34].

There has been active research in recent years in the area of preprocessing of OFDM signals for PAPR reduction (data predistortion) [35, 36] and signal predistortion [34]. This work follows a third approach: If some non-linear distortion at the transmitter is allowed, the requirements on the RF frontend can be relaxed. Information theory shows that signal clipping in an OFDM transmitter only results in a marginal reduction of channel capacity [37], which motivates the search for powerful receive algorithms. Based on *Maximum-Likelihood* (ML) detection, a suitable algorithm is derived.

5.1. System and Channel Model

The system model used throughout this section represents a simplified, discrete time, baseband equivalent OFDM system. A vector $\mathbf{X} = [X_0, X_1, \ldots, X_{N-1}]^{\mathrm{T}}$ of length N is formed at the transmitter, and $X_k \in \mathcal{S} \forall k \in N, 0 \leq k \leq N-1$, where the symbol set $\mathcal{S} = (S_0, S_1, \ldots, S_{M-1})$ contains all $M = 2^p, p \in N$ possible complex transmit symbols.

$\mathbf{X}$ is then converted to the time domain vector $\mathbf{x} = [x_0, x_1, \ldots, x_{N-1}]^{\mathrm{T}}$ by means of an *Inverse Discrete Fourier Transform* (IDFT) of length N. The elements of $\mathbf{x}$ are approximately complex Gaussian distributed, with variance P_x. Typically, $\mathbf{x}$ will exhibit significant envelope fluctuations because of constructive and destructive superposition of the elements of $\mathbf{X}$. The time domain vector is then distorted by a non-linear function $f(\cdot)$ to deliver $\mathbf{z} = [z_0, z_1, \ldots, z_{N-1}]^{\mathrm{T}}$. Throughout this paper, the baseband equivalent memoryless non-linearity $f(\cdot)$ is assumed to be a soft limiter, which distorts the magnitude but not the phase of the elements of $\mathbf{x}$. This models the baseband equivalent of an ideally predistorted non-linear PA. The magnitude $r_{z,k} = |z_k|$ is then given by

$$r_{z,k}(r_{x,k}) = \begin{cases} r_{x,k} & r_{x,k} \leq A \\ A & r_{x,k} > A \end{cases}. \tag{20}$$

A is the clipping level of the non-linear device.

After the non-linearity, a vector $\mathbf{n} = [n_0, n_1, \ldots, n_{N-1}]^{T}$ of complex AWGN samples further corrupts $\mathbf{z}$ to yield

$$\mathbf{y} = \mathbf{z} + \mathbf{n}. \tag{21}$$

This system model is shown in Figure 7. The complex Gaussian random variables n_k are assumed to be zero-mean with variance P_n and uncorrelated. The

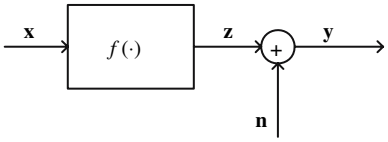

Fig. 7. System and channel model.

Input Power Backoff for the soft limiter device is given by

$$\mathrm{IBO} = A^2/P_x. \tag{22}$$

5.2. Detection Algorithm

In the following, it is assumed that the non-linear function f is known at the receiver. This is reasonable when the digital baseband signal at the transmitter is clipped deliberately. The ideal ML detector for the communications system under consideration forms all possible transmit vectors $\hat{\mathbf{X}}_i$, where $0 \leq i \leq M^N-1$. Then, these vectors are converted to the time domain and distorted by f, resulting in the vectors $\hat{\mathbf{z}}_i$. Finally, the distance of each $\hat{\mathbf{z}}_i$ to the received vector $\mathbf{y}$ is computed, and the one with minimum distance is selected. To summarize, the ML detector solves the following problem:

$$\hat{\mathbf{X}} = \arg\min_{\hat{\mathbf{X}}_i} \left|\left|\mathbf{y} - f\left[\mathrm{IDFT}\{\hat{\mathbf{X}}_i\}\right]\right|\right|^2. \tag{23}$$

It is apparent that such a detector is prohibitively complex for practical values of N and M. Therefore, it is desirable to reduce its complexity. The following approach is proposed: Instead of generating all possible hypotheses for the vector $\mathbf{X}$ in parallel, we look for the symbol which minimizes the above distance metric in the time domain for each element of $\mathbf{X}$ sequentially. The complete detection algorithm then consists of the following steps:

(1) Convert the received time domain vector $\mathbf{y}$ into the frequency domain vector $\mathbf{Y}$ by means of a *Discrete Fourier Transform*. Then, quantize $\mathbf{Y}$ according to the decision boundaries corresponding to the symbol alphabet $\mathcal{S}$ (hard detection). This operation is denoted by

$$\hat{\mathbf{X}}_1 = \mathrm{dec}(\mathbf{Y}) \tag{24}$$

and delivers a first estimate of $\mathbf{X}$.

(2) Generate M new frequency domain vectors $\hat{\mathbf{X}}_{1,1}^{(0)}$ to $\hat{\mathbf{X}}_{1,M}^{(0)}$ based on $\hat{\mathbf{X}}_1$ by inserting all possible symbols from $\mathcal{S}$ as the first vector element. The superscript denotes the index of the element which is varied.

(3) Compute the distances

$$d_{1,m}^{(0)} = \left|\left|\mathbf{y} - f\left[\mathrm{IDFT}\{\hat{\mathbf{X}}_{1,m}^{(0)}\}\right]\right|\right|^2 \tag{25}$$

for $1 \leq m \leq M$. Choose the symbol which results in the smallest distance.

(4) Repeat steps 2 and 3 for all N elements of $\hat{\mathbf{X}}_1$. Thus, the symbol decisions are refined sequentially.

When no non-linear distortion is present, this algorithm is equal to the complete ML solution, because the DFT and IDFT are orthogonal transforms, and reducing a possible error term in the frequency domain inevitably results in a reduced time domain error. The non-linear function f destroys orthogonality, which makes the above algorithm suboptimum. However, it reduces the exponential ML complexity to linear complexity. MN hypotheses are tested, and further simplifications are possible. For example, a subset of less than M symbols could be tested per subcarrier. The loss of orthogonality also implies that the order, in which the subcarriers are tested, can affect the convergence behavior. Furthermore, several iterations of the whole algorithm can improve performance.

5.3. Performance Results

The algorithm was tested with uncoded QPSK and 16-QAM transmission and $N = 64$. No guard or pilot subcarriers were simulated, and the transmission channel model was AWGN. The soft limiter backoff was set at 0 dB, modelling an extremely severe clipping. Figure 8 shows the performance of a QPSK system for this IBO. It can be seen that the performance with clipping and sequential *Mean-Square Error* (MSE) reduction actually surpasses linear AWGN performance in certain E_b/N_0 regions. Two effects are responsible for this behavior: First,

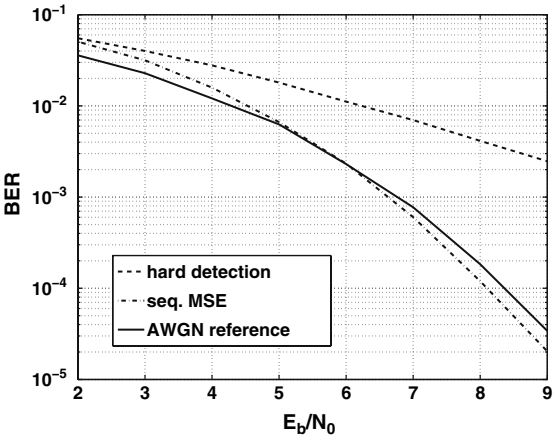

Fig. 8. Performance of sequential MSE reduction for QPSK modulation.

clipping reduces the transmit power by a factor of $\beta = 1 - e^{-\mathrm{IBO}}$, which results in a rescaling of the E_b/N_0 axis for a fair comparison. For an IBO of 0 dB, the resulting SNR gain is 2 dB. Second, the non-linear distortion introduces dependencies between the frequency domain symbols, which help in recovering the correct symbols.

While the algorithm offers good performance, it is only suitable for small numbers of subcarriers because of its computational complexity. Future work includes further reduction of complexity and soft detector implementations, preferably coupled with a soft in-soft out decoder. The following subsection focuses on a different approach, which can be used for large OFDM systems as well.

5.4. Iterative Correction based on Hard Detection

Instead of approximating the complete search, an alternative is to estimate the clipped portion of the signal. Tellado et al. [38], as well as Chen and Haimovich [39], proposed to compute the clipping noise term according to the Bussgang decomposition [40]. This noise term is then subtracted in the frequency domain according to the following steps (see the sketch of the receiver algorithm for the uncoded case in Figure 9):

(1) compute an estimate of the transmit sequence $\hat{\mathbf{x}}$ based on hard decisions $\hat{\mathbf{X}}$ derived from the demodulated equalized symbol vector $\mathbf{Y}$.
(2) calculate the difference $\mathbf{d} = \alpha\hat{\mathbf{x}} - f(\hat{\mathbf{x}})$ between the clipped sequence $\hat{\mathbf{z}} = f(\hat{\mathbf{x}})$ and the attenuated unclipped sequence $\alpha\hat{\mathbf{x}}$.
(3) add the Fourier transform $\mathbf{D}$ of this difference as a spectral correction to the demodulated symbols.

These steps can be applied iteratively to improve the reconstruction of the time domain sequence and in turn the hard symbol decisions, either until convergence or until a maximum number of iterations is reached. Note the low complexity of the algorithm, even for large numbers of OFDM subcarriers.

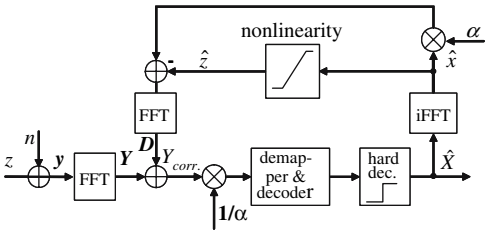

Fig. 9. Iterative clipping correction as proposed in [38, 39].

5.5. Performance over AWGN Channel

As before, we assume that using predistortion the non-linearity can be modeled as a soft limiter and that its characteristics (the IBO value) are known at the receiver.

The parameter space with IBO, alphabet size, number of subcarriers, number of iterations and channel conditions is relatively large. We chose a severe clipping situation and intermediate constellation size as a point of reference, namely 16-QAM with an IBO of 0 dB.

The correction capability for different IBO was studied in the numerical experiment shown in Figure 10. Comparing the zero forcing solution (just a linear scaling according to the Bussgang decomposition) to the first and third iteration of the algorithm, we notice that for all IBO levels the performance is improved by two orders of magnitude. Similarly the increase of the back off from 0 to 2 dB reduces the error floor by two orders of magnitude (BER $= 2 \times 10^{-4} \rightarrow 2 \times 10^{-6}$).

Interestingly, the performance of the clipping correction rather strongly depends on the number of subcarriers. That was already observed in [38], where two cases differing by a factor of two were compared. Again the severe clipping with IBO = 0 dB is studied in Figure 11. While the differences are small for the first iteration, they magnify with increasing iteration number. We attribute this to the fact that for a larger

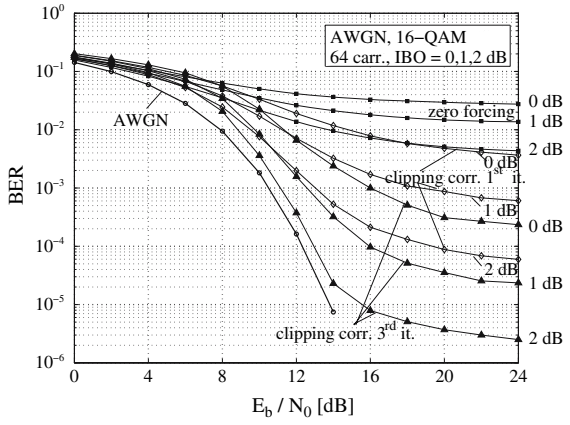

Fig. 10. Iterative clipping correction for different input power backoff for 16-QAM transmitted over an over AWGN channel.

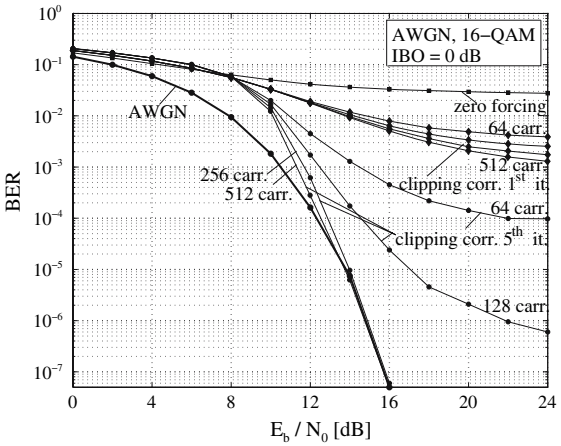

Fig. 11. Iterative clipping correction for different numbers of subcarriers (IBO 0 dB, 16-QAM, AWGN).

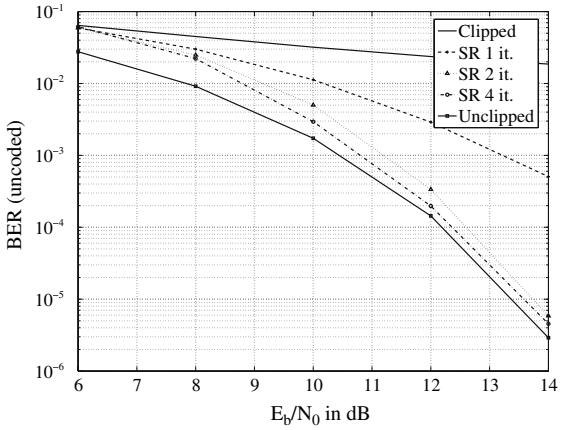

Fig. 12. Iterative clipping correction with clipping and filtering at the transmitter (IBO 0 dB, 16-QAM, AWGN).

number of subcarriers the Gaussian assumption in the Bussgang decomposition becomes more precise.

Another important dependence is of course the constellation size. Clearly, sensitivity to clipping should increase from QPSK to 16-QAM and 64-QAM. A performance example illustrating this and the effect of the employment of coding can be found in [41].

Lastly, the combination of s simple PAPR reduction algorithm and clipping correction shall be mentioned. It is well known that clipping and filtering in the digital baseband of an OFDM transmitter can reduce the PAPR significantly. We tested this approach with an FFT size of 1024, where 616 carriers were used for transmission, resulting in an oversampling factor of about 1.66. The time domain OFDM signal was clipped and transformed back to the frequency domain. The zero carriers were set to zero again, and the signal was converted to the time domain again for actual transmission. The PAPR of the signal is reduced by about 5.5 dB, and the performance for an IBO of 0 dB and 16-QAM with clipping correction is shown in Figure 12.

6. CONCLUSIONS

In this paper, we considered several problems that arise due to the presence of impairments in the analog RF chain of transceivers for wireless communications systems: jitter, phase noise, I/Q-imbalance and non-linear PA. We presented some evaluation methods to analytically evaluate the resulting performance losses as well as baseband processing algorithms that allow for alleviation or even total compensation of these deteriorating effects.

For simplicity, all effects have been considered separately. The joint treatment of all effects is beyond the scope of this paper. Other effects such as DC offset, sampling frequency offset, symbol timing errors have not been considered, it is referred to the literature [42–44].

We have shown that by knowing the statistical properties of impairments in the analog front-end and using powerful digital baseband processing, future wireless communications systems may be able to some extend to actually *live with Dirty RF*. We are hence able to extend the transmission rate by joint optimization of RF components and baseband processing – opening the path for high performance devices at reasonable cost.

REFERENCES

1. R. H. Walden, Analog-to-digital converter survey and analysis, *IEEE Journal of Selected Areas in Communication*, Vol. 17, pp. 539–550, Apr. 1999.
2. H. Kobayashi, M. Morimura, K. Kobayashi, and Y. Onaya, Aperture Jitter Effects in Wideband ADC Systems, *Proc. 6th IEEE International Conference on Electronics, Circuits and Systems (ICECS '99), (Pafos, Cyprus)*, pp. 1705–1708, Sept. 1999.
3. S. S. Awad, Analysis of accumulated timing-Jitter in the time domain, *IEEE Transactions on Instrument and Measurement*, vol. 47, pp. 69–73, Feb. 1998.
4. N. Dalt, M. Harteneck, C. Sandner, and A. Wiesbauer, On the Jitter requirements of the sampling clock for analog-to-digital converters, *IEEE Transactions On Circuits Systems-I,* Vol. 49, No. 9, pp. 1354–1360, 2002.

5. N. Dalt, Effect of jitter on asynchronous sampling with finite number of samples, *IEEE Transactions On Circuits Systems-II: Express Briefs,* Vol. 51, No. 12, pp. 660–664, 2004.
6. M. Löhning and G. Fettweis, The effects of aperture jitter and clock jitter in wideband ADCs, *Proc. International Workshop on ADC Modelling and Testing (IWADC 2003), (Perugia, Italy)*, pp. 187–191, 08–10 Sept. 2003.
7. M. Löhning and G. P. Fettweis, The effects of aperture Jitter and Clock Jitter in Wideband ADCs, Special Issue of the *International Journal Computer Standards and Interfaces (CS&I)*, Vol. 29, No. 1, 2006, in press.
8. M. Löhning, Analyse und Modellierung der Effekte von Abtast-Jitter in Analog-Digital-Wandlern. PhD thesis, Technische Universität Dresden, Dresden, Germany, 2006.
9. G. Fettweis, M. Löhning, D. Petrovic, M. Windisch, P. Zillmann, and E. Zimmermann, Dirty RF, *Proceedings of the 11th Wireless World Research Forum (WWRF11), (Oslo, Norway), 10–11*, June 2004.
10. A. Papoulis and S. U. Pillai, *Probability, Random Variables and Stochastic Processes*, 4th ed., McGraw-Hill Education, 2002.
11. A. Demir, A. Mehrotra, and J. Roychowdhury, Phase noise in oscillators: A unifying theory and numerical methods for characterization, *IEEE Transactions On Circuits Systems-I,* Vol. 47, No. 5, pp. 655–674, 2000.
12. J. A. Cherry, and W. M. Snelgrove, Clock Jitter and quantizer metastability in continuous-time delta–sigma modulators, *IEEE Transactions On Circuits Systems-II,* Vol. 46, No. 6, pp. 661–676, 1999.
13. G. Matz and F. Hlawatsch, Time-Varying Power Spectra of NonStationary Random Processes. In B. Boashash (Ed.), *Time-Frequency Signal Analysis and Processing: A Comprehensive Reference*, 1st ed., Elsevier, Oxford, UK, pp. 400–409, 2003.
14. A. W. Rihaczek, Signal energy distribution in time and frequency, *IEEE Transactions on Information Theory*, Vol. IT–14, pp. 369–374, May 1968.
15. J. C. O'Neill and W. J. Williams, Shift covariant time-frequency distributions of discrete signals, *IEEE Transactions on Signal Processing*, Vol. 47, pp. 133–150, Jan. 1999.
16. A. Armada, Understanding the effects of phase noise in orthogonal frequency division multiplexing (OFDM), *IEEE Transactions on Broadcasting*, Vol. 47, pp. 153–159, June 2001.
17. P. Robertson and S. Kaiser, Analysis of the effects of phase noise in OFDM systems, *Proc. ICC*, 1995.
18. S. Wu and Y. Bar-Ness, A phase noise suppression algorithm for OFDM-Based WLANs, *IEEE Communications Letters*, Vol. 6, No. 12, pp. 535–537, Dec. 2002.
19. D. Petrovic, W. Rave, and G. Fettweis, Phase noise suppression in OFDM including intercarrier interference, *Proc. Intl. OFDM Workshop (InOWo) 03*, pp. 219–224, 2003.
20. D. Petrovic, W. Rave, and G. Fettweis, Intercarrier interference due to Phase Noise in OFDM – estimation and suppression, *Proc. IEEE VTC Fall*, Sept. 2004.
21. A. Oppenheim and R. Schafer, *Discrete-Time Signal Processing*. Prentice-Hall Inc., 1989.
22. IEEE, Part11: Wireless LAN Medium Access Control (MAC) and Physical Layer (PHY) Specifications. High-speed Physical Layer in the 5 GHz Band, *IEEE Std 802.11a-1999*, 1999.
23. B. Razavi, Design considerations for direct-conversion receivers, *IEEE Transactions On Circuits Systems-II,* Vol. 44, No. 6, pp. 428–435, 1997.
24. J. Crols, and M. S. J. Steyaert, Low-IF topologies for high-performance analog front ends of fully integrated receivers, *IEEE Transactions On Circuits Systems-II,* Vol. 45, No. 3, pp. 269–282, 1998.
25. J. P. F.Glas, Digital I/Q imbalance compensation in a Low-IF receiver. in *IEEE Global Communications Conference*, Vol. 3, pp. 1461–1466, 1998.
26. S. Simoens, M. de Courville, F. Bourzeix, and P. de Champs, New I/Q imbalance modeling and compensation in OFDM systems with frequency offset, *Proc. IEEE PIMRC 2002*, Vol. 2, pp. 561–566, Sept. 2002.
27. A. Schuchert, R. Hasholzner, and P. Antoine, A novel IQ imbalance compensation scheme for the reception of OFDM signals, *IEEE Transactions on Consumer Electronics,* Vol. 47, No. 8, pp. 313–318, 2001.
28. M. Windisch and G. Fettweis, Blind I/Q imbalance parameter estimation and compensation in low-IF receivers, *Proc. 1st Intl. Symposium on Control, Communications and Signal Processing (ISCCSP 2004), (Hammamet, Tunisia), 21–24 Mar. 2004.*
29. M. Windisch and G. Fettweis, Standard-Independent I/Q imbalance compensation in OFDM direct-conversion receivers, *Proc. 9th Intl. OFDM Workshop (InOWo), (Dresden, Germany)*, pp. 57–61, 15–16 Sept. 2004.
30. M. Windisch and G. Fettweis, Preamble design for an efficient I/Q imbalance compensation in OFDM direct-conversion receivers, *Proc. 10th International OFDM Workshop (InOWo), (Hamburg, Germany)*, pp. 94–98, 2005.
31. M. Windisch and G. Fettweis, On the performance of standard-independent I/Q imbalance compensation in OFDM direct-conversion receivers, in *Proc. 13th European Signal Processing Conference (EUSIPCO), (Antalya, Turkey), 4–8 Sept. 2005.*
32. IEEE, Part11: Wireless LAN Medium Access Control (MAC) and Physical Layer (PHY) specifications, *IEEE Std 802.11a-1999*, 1999.
33. A. R. S. Bahai and B. R. Saltzberg, *Multi-Carrier Digital Communications – Theory and Applications of OFDM*. Kluwer Academic/Plenum, 1999.
34. S. C. Cripps, *RF Power Amplifiers for Wireless Communications*. Artech House, 1999.
35. D. J. G. Mestdagh, and P. M. P. Spruyt, A method to reduce the probability of clipping in DMT-based transceivers, *IEEE Transactions on Communication,* Vol. 44, No. 10, pp. 1234–1238, 1996.
36. S. Shepard, J. Orriss, and S. Barton, Asymptotic limits in peak envelope reduction by redundancy coding in OFDM modulation, *IEEE Transactions on Communication,* Vol. 46, No. 1, pp. 5–10, 1998.
37. P. Zillmann and G. Fettweis, On the capacity of multicarrier transmission over non-linear channels, *Vehicular Technology Conference, Stockholm, 29 May–1 June, 2005.*
38. J. Tellado, L. Hoo, and J. M. Cioffi, ML detection of nonlinearly distorted multicarrier symbols by iterative decoding, *IEEE Transactions on Communication,* Vol. 51, No. 2, pp. 218–228, 2003.
39. H. Chen, and A. M. Haimovich, Iterative estimation and cancellation of clipping noise for OFDM, *IEEE Communications Letters,* Vol. 7, No. 7, pp. 305–307, 2003.
40. A. Papoulis, *Probability, Random Variables and Stochastic Processes*, 3rd ed. McGraw-Hill Inc., 1991.
41. W. Rave, P. Zillmann, and G. Fettweis, Iterative correction and decoding of OFDM signals affected by Clipping, in *Proc. MC-SS 2005, Germany*, pp. 443–452, 14–16 Sept. 2005.
42. J. Heiskala and J. Terry, *OFDM Wilreless LANs: A Theoretical and Practical Guide*. SAMS, 2002.
43. M. Speth, S. Fechtel, G. Fock, and H. Mehr, Optimum receiver design for wireless broad-band systems using OFDM – Part I, *IEEE Transactions on Communication,* Vol. 47, No. 11, pp. 1668–1677, 1999.
44. T. Pollet, P. Spruyt, and M. Moeneclaey, The BER performance of OFDM systems using non-synchronized sampling, *Proc. GLOBECOM*, pp. 253–257, Nov. 1994.

Gerhard Fettweis studied electrical engineering at the Aachen University of Technololgy (RWTH) in Germany and earned a PhD degree in 1990. From 1990 to 1991, he was Visiting Scientist at the IBM Almaden Research Center in San Jose, CA, developing signal processing innovations for IBM's disk drive products. From 1991 to 1994, he was a Scientist with TCSI Inc., Berkeley, CA, responsible for signal processor development projects for mobile phone chip-sets. Since September 1994 he holds the Vodafone Chair at the Technische Universität in Dresden, Germany. In addition he cofounded Systemonic as CTO in 1999, which was successfully acquired by Philips Semiconductor in December 2002. Now he is Chief Scientist of Philips Semiconductors BL-C. In 2000, a second start-up was spun-out of the Vodafone Chair: Radioplan delivers products and professional services related to 2.5G, 3G and 4G network development, planning and optimization. In 2003, a third startup was spun out: Signalion provides leading edge consulting, engineering & prototype development for signal processing and communications systems. The forth startup, InCircuit (2004) delivers custom electronic circuit solutions for signal processing products. The fifth startup, Dresden Silicon (2005), delivers media codec circuits and solutions for mobile devices. Gerhard Fettweis' research at the Vodafone Chair focuses on new wireless communications systems for cellular and short range networks, and their hardware/software implementation.

Michael Löhning was born in Stralsund, Germany in 1973. He received his M.Sc./Dipl.-Ing. and his Ph.D. degrees in Electrical Engineering from the Dresden University of Technology, Germany, in 1999 and 2006, respectively. In 1999, he joined the Vodafone Chair Mobile Communications Systems at the University of Dresden as a research associate. His research was on software radio based front-end architectures for reconfigurable mobile communications systems, specifically on digital filter banks, AD-converter banks, and most prominent on jitter effects in AD converters. In 2003, he co-founded Signalion – a start-up that provides leading edge consulting, engineering & prototype development for signal processing and communications systems. Since 2005 he has been working with Signalion as a senior system architect.

Denis Petrovic was born in Belgrade, Yugoslavia in 1976. He received the Dipl.-Ing. degree in 2001 from the University of Belgrade, Yugoslavia, and the Ph.D. degree in electrical engineering in 2005 from Technische Universität Dresden, Germany. Before starting a Ph.D. at Technische Universität Dresden he was envolved in several research projects at California Institute of Technology, Pasadena; Vodafone Chair Mobile Communications Systems, Technische Universität Dresden and Ericsson Eurolab Deutschland, Nueremberg, Germany. He is currently working as a research scientist at Vodafone Chair Mobile Communications Systems, Technische Universität Dresden. His research interest include synchronization in WLAN, coding and MIMO.

Marcus Windisch received his Dipl.-Ing. degree from Technische Universität Dresden, Germany in 2002 after studies at TU Dresden and at the University of Wisconsin (UW), Madison, WI. During his studies, he spent 6 months with the DaimlerChrysler

research center in Ulm, Germany, working on wireless car-to-car communications based on Mobile IPv6. In 2002, he joined the Vodafone Chair Mobile Communications Systems at TU Dresden. His research interests include the design of wireless communications systems and the digital compensation of analog impairments in advanced transceiver architectures, with special focus on I/Q imbalance.

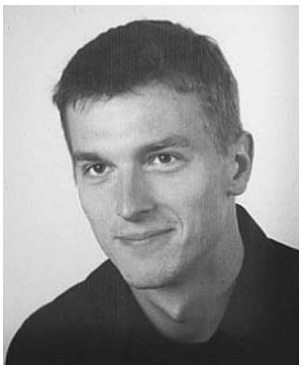

Peter Zillmann holds a M. Sc. EE degree from New Jersey Institute of Technology (NJIT), Newark, NJ, and a Dipl.-Ing. degree from Technische Universität Dresden, Germany. In 2002, he spent 6 months with Systemonic AG, Dresden, now Philips Semiconductors Dresden, working on wireless LAN transceivers. In 2003, he joined the Vodafone Chair Mobile Communications Systems at TU Dresden as a research associate. His research interests include wireless communications, digital signal processing, and non-linear systems, as well as the design of wireless multimedia networks.

Wolfgang Rave was born in Stuttgart, Germany, in 1960. He received the Dipl.-Ing. and Ph.D. degrees in Materials Science for Electrical Engineering from the University of Erlangen-Nürnberg in Materials Science of Electrical Engineering in 1985 and 1990, respectively. After postgraduate work at the university of Paris-Sud and the Institut für Festkörper- und Werkstoffforschung Dresden on numerical micromagnetics he joined the Vodafone Chair for Mobile Communications in 1999. His current research interests include OFDM and MIMO transmission techniques with a special interest on iterative detection and decoding.